INT. J. REMOTE SENSING, 2002, VOL. 23, NO. 6, 1075–1094

Effects of farming works on soil surface bidirectional reflectance measurements and modelling

J. CIERNIEWSKI

Adam Mickiewicz University, Institute of Physical Geography, Fredry 10, 61-701 Poznan, Poland; e-mail: c´ernje@amu.edu.pl

M. VERBRUGGHE

INRA, Bioclimatologie, Site Agroparc, 84914 Avignon, France

A. MARLEWSKI

Poznan University of Technology, Institute of Mathematics, Piotrowo 3a, 60-965 Poznan, Poland

(*Received 29 May 2000; in final form 19 February 2001*)

Abstract. A model describing the directional reflectance in the optical domain from cultivated soil surfaces, taking into account their farming direction, is presented in the paper. It is discussed on the background of the directional reflectance measurements of soil surfaces, being effects of farming works preparing the soil for colza sowing. The model considers a soil surface as equal-sized opaque spheroids of definite shape and size dispersed in a net of squares on a freely sloping plane. They are absorbed into the plane having with their tops at a height above it. Different values for this height, along and across the soil cultivation direction, are parameters which express the variation of soil surface irregularities caused by furrowed farming treatments. The structure is illuminated by direct solar and diffuse light. Wave energy is reflected from it taking into account the diffuse and the specular components. A set of geometrical parameters of the structure, the equivalent of the real rough soil surface, makes it possible to predict the soil directional reflectance in any illumination and viewing conditions. It was applied to trace the influence of the direction of furrows, caused by a seeder, on the soil bidirectional reflectance.

1. Introduction

The reflectance of soil surfaces in the optical domain strongly depends on the geometry of their illumination and viewing. Irregularities of the soil surface, caused by the soil texture, aggregates and a micro-relief configuration, produce shadow areas, where the solar beams do not directly reach the surface. Wave energy leaving the shaded areas is many orders of magnitude smaller than energy coming from the Sun. Cultivated bare soils with dominant diffuse features usually seem to be the brightest from the direction which gives the lowest proportion of shaded fragments. Those soil surfaces usually display a clear backscattering character with a reflectance

International Journal of Remote Sensing
ISSN 0143-1161 print/ISSN 1366-5901 online © 2002 Taylor & Francis Ltd
http://www.tandf.co.uk/journals
DOI: 10.1080/01431160110071897

peak towards the Sun position and decreasing reflectance in the direction away from the peak.

The intensity of soil surface shadowing depends on the general and the micro-relief configuration of the soil surface slopes in relation to incident rays. Most geometrical soil directional reflectance models that have been proposed predict soil reflectance based on the assumption that shadowing of soil irregularities has a greater influence than the scattering properties of a soil material at the micro-scale. Soil aggregates in the model of Norman *et al.* (1985) were simulated by cuboids. The height of soil surfaces in the Monte Carlo reflectance model of Cooper and Smith (1985) varied periodically with the cosine function in one or two directions. The models of Cierniewski (1987) and Irons *et al.* (1992) describe soil aggregates by regularly spaced equal-sized opaque spheres, while Cierniewski and Verbrugghe's models (1994) simulate them by spheroids of a defined proportion of their vertical to horizontal radii. All the models assume only perfectly diffuse reflection from the sunlit soil fragments. Improved versions of the models, describing bidirectional reflectance from non-directional rough soil surface with regular dispersed soil aggregates, also take into account specular features of the soil material (Cierniewski *et al.* 1996, Cierniewski and Verbrugghe 1997, Cierniewski 1999).

This work concentrates on the bidirectional reflectance modelling from cultivated soil surfaces with soil aggregates dispersed either randomly or directionally. Previous geometrical models had been used to predict the normalized reflectance of furrowed cultivated soils, and assumed that their soil material is perfectly diffuse objects (Cierniewski *et al.* 1998). The newest model, applied at present to analyse effects of farming works on soil bidirectional reflectance, takes into account the diffuse, as well as the specular components of energy in the optical domain leaving soil surfaces. The model uses virtual surfaces to predict the directional reflectance of cultivated soils in any illumination and viewing conditions. Its operation is tested on a heavy soil prepared for sowing, using agricultural tools like a harrow, a seeder and a roller.

Knowledge of the directive reflectance behaviour of cultivated soil surfaces is especially useful for their interpretation using data obtained by air-borne and satellite wide field-of-view sensors and the narrow FOV sensors tilted at different angles (Ott *et al.* 1984, Barnsley 1994). The data collected in different illumination and viewing conditions need corrections to a standardized form before classification procedures. It can eliminate soil interpretation errors that are only the results of dissimilarity of those conditions.

2. The experiment

2.1. *Soil surfaces*

The experiment was conducted on a field of a bare soil developed from loamy alluvium (table 1) of the Rhône delta, situated in the south of France near Saint-

Table 1. Properties of studied soil surfaces.

		Mechanical fraction content (%)		
Organic matter content (%)	Texture	Sand (2 mm–50 μm)	Silt (50 μm–2 μm)	Clay (<2 μm)
1.75	Loam	43.9	40.2	15.9

Remy (43°45′N, 4°55′E) (figure 1). The directional reflectance of soil surfaces at different roughness states, the results of farming works successively preparing the soil for colza *Brassica napus oleifera* sowing, were collected from 9 to 18 September 1998. Each of the soil surfaces deeply ploughed, harrowed and rolled, furrowed by the seeder and finally rolled, were photographed on the background of a special frame. The frame, with 5 cm × 5 cm wire nets, made it easier to characterize the size of the soil surface aggregates. Furthermore, effects of the heavy 40 mm rain on the direction reflectance of the soil surfaces were observed.

2.2. *Soil bidirectional reflectance measurements*

The bidirectional reflectance of the soil surfaces were measured by the three-channel radiometer CIMEL simulating the SPOT HRV bands. The instrument, with a 12° FOV, records radiance of a target in the following wavelength bands: 500–590 nm (XS1), 610–680 nm (XS2) and 790–890 nm (XS3). The apparatus was fixed on a goniometric support, which enabled us to observe the target from the distance of 2 m at 15 view zenith angles from 70° towards the Sun through the nadir (0°) to 70° away from the Sun at 10° increments. The surface radiance data were collected along the solar principal plane SPP and other planes situated in relation to the Sun direction at angles ϕ_v. The direction of the furrows of the harrowed soil surfaces has been expressed by the horizontal ϕ_r angle, measured with respect to the solar beams direction. The 17 three-channel measurements of the radiance were taken in a given measurement plane, defined by the ϕ_v angle, at a given solar zenith angle θ_s, because each series of the 15 measurements, mentioned above, was preceded and ended by additional measurements taken from the nadir. All these radiance data at one measurement plane were recorded in about five minutes.

The measurements were acquired on air-dried soil surfaces under clear sky conditions at the solar zenith angles θ_s, illumination ϕ_r and view ϕ_v angles arranged as specified in table 2. The speed of the successively performed farming works

Figure 1. General view of the studied soil surfaces.

Table 2. Values of the solar zenith angle θ_s, the horizontal angle between vertical viewing plane and the Sun direction ϕ_s and the horizontal angle between the cultivation direction and the Sun direction angles ϕ_r for which the luminance measurements for the soil surface were collected.

Date	Farming works	Symbol	$\theta_s/\phi_v/\phi_r$				
9 September 1998	Harrowed and rolled	S09	38.7/0/0	47.6/0/0	62.8/0/0		
9 September 1998	Ploughed	R09	37.9/0/0	45.5/0/0	60.1/0/0		
10 September 1998	Rolled after sowing	S10	55.8/0/0	45.0/0/0			
10 September 1998	Furrowed by the seeder	F10	67.1/0/39.8	58.1/0/28.4	47.2/0/9.8	39.9/0/55.0	
10 September 1998	Furrowed by the seeder	F10	38.2/51.3/38.7	45.0/15.5/74.3	49.5/5.0/80.0	59.0/10.0/85.5	66.3/18.5/108.5
14 September 1998	Furrowed by the seeder, after rain	Fr14	40.8/0/51.0	46.6/0/74.2	52.5/0/87.2	63.3/0/76.8	
14 September 1998	Ploughed, after rain	Rr14	44.8/0/0	49.3/0/0	55.6/0/0	66.3/0/0	
14 September 1998	Rolled, after rain	Sr14	41.4/0/0	48.2/0/0	53.5/0/0	64.7/0/0	
16 September 1998	Furrowed by the seeder, after rain	Fr16	47.0/86.9/3.1	42.4/85.0/5.0			
18 September 1998	Furrowed by the seeder, after rain	Fr18	54.6/3.1/86.9				

determined the numbers of the spectral measurement sets collected for the individual soil surfaces.

2.3. *The model*

The model predicts the directional distribution of electromagnetic radiation in the optical domain, reflected from soil surfaces in farming lands. Roughness of the soil surfaces is caused by irregularities of soil aggregates, of different size and shape, dispersed in accordance with the direction of soil preparation for any agricultural treatment, creating a kind of furrow.

Equal-sized opaque spheroids of horizontal, a, and vertical, b, semiaxis were regularly dispersed on a slope such that their centres are in a square grid of interval d (figure 2). The d corresponds with the distance between successive rows of the furrows. The simulated soil slope determines two planes, parallel to each other, sloping at angle ε. The lower plane is described by lines lying in the bottom of the furrows, while the higher determines a ground of irregularities on the top of the furrows. The spheroids absorbed into the higher slope plane with their tops projecting at height t_r above the ground characterized the soil surface irregularities along the direction of the soil farming, while the spheroids absorbed into the lower slope plane,

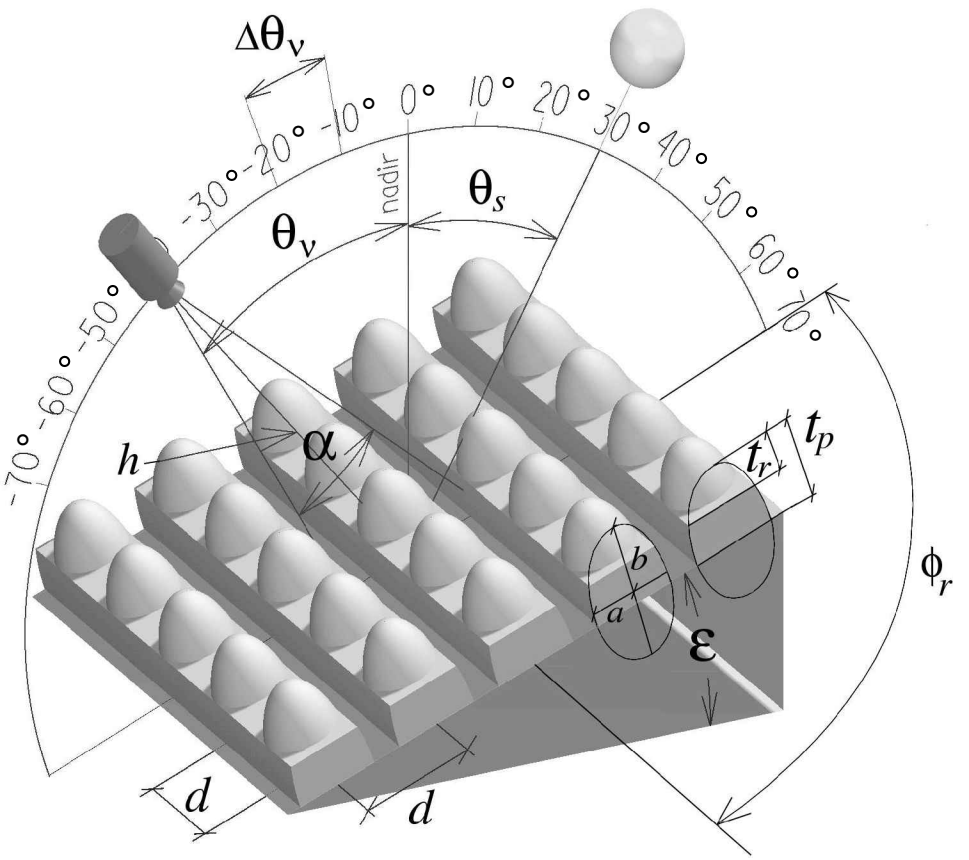

Figure 2. Schema of the model representation and its illumination and observation parameters.

with their tops at height t_p above the plane, describe the surface irregularities perpendicular to the direction. The soil surface irregularities, lower along the farming direction than perpendicular to it, are expressed by lower values of the height t_r than t_p.

When $t_r = t_p$ both the planes mentioned above cover each other and the model can simulate the soil reflectance from non-directional rough soil surface with regular dispersed soil aggregates.

The geometrical structure is illuminated by the direct solar beams at a zenith angle θ_s and diffuse skylight, described by the factor f_{di}. The f_{di}, defined as part of the direct solar beam energy, approximates a reflectance effect from soil surfaces illuminated only by the diffuse light component.

A sensor is suspended over the simulated soil surface. It observes the surface along the SPP at zenith angles θ_v, at the $\Delta\theta_v$ increments in forward scattering and backscattering directions, described by negative and positive values of the θ_v, respectively. The sensor with field-of-view that defines the angle α is located at a distance h away from the observed surface. The model assumes that the total energy coming to the sensor after reflection from the simulated soil surface is a proper weight mean calculated along many profiles situated parallel to the SPP inside the sensor FOV. The calculation along the SPP is executed twice, assuming that the SPP is first parallel to the farming direction and second perpendicular to the direction. In the first step of the calculation in a given profile, the position of all the border points between the directly illuminated and shaded fragments of the geometrical structure is computed.

An amount of the wave energy coming directly to the illuminated individual facet fa of the geometrical structure, the ellipse and the soil slope between the ellipses, defines the factor $Ei_v{}^{\propto}{}_{f_a}$:

$$Ei_v{}^{\propto}{}_{f_a} = \cos\theta_s \cos\beta + \sin\beta + \sin\theta_s \cos(\phi_r - \phi_s) \tag{1}$$

where: β is the slope angle of the facet, and ϕ_r and ϕ_s are the azimuth angles describing the position of the facet and the Sun, respectively. The value of this factor $Ei_v{}^{\propto}{}_{f_a}$, equals the cosine of the incidence angle γ of the direct sun beams to the facet, measured from its normal. The energy leaving the directly illuminated facets $Ei_v{}^{\uparrow}{}_{f_a}$ is directly proportional to the energy incident on it $Ei_v{}^{\propto}{}_{f_a}$. The $Ei_v{}^{\uparrow}{}_{f_a}$ is in part perfectly diffused, and in part reflected as from the specular reflection. The length of the reflected energy vector to a given direction θ_v is the sum of the length of the two vectors: of the perfectly diffused energy $Edi_{\theta_v}{}^{\uparrow}{}_{f_a}$ and the energy specularly reflected $Esp_{\theta_v}{}^{\uparrow}{}_{f_a}$ (figure 3). The length of the vector $Esp_{\theta_v}{}^{\uparrow}{}_{f_a}$, describing unpolarized light, depends on polarization $Fp_{(\gamma)}$ of the reflected light $Ei_v{}^{\propto}{}_{f_a}$ at the γ_i angle. The $Fp_{(\gamma)}$ is calculated from Fresnel's equations using the refractive index n of soil surface. The vector of the energy specularly reflected is oriented in such a way that the angle of incidence γ_i equals the angle of reflection γ_r. As the vector of the quasi-specular reflected energy, it is visible inside the limited angle range described by the 2∂ angle around the direction of reflection.

The diffuse light component $Esk^{\propto}{}_{f_a}$ reaches the soil surface fragments directly illuminated by the sun beams, as well as the shaded fragments. Its amount is limited by the presence of adjoining spheroids (ellipses in profile), which reduce the amount of the diffuse energy by comparison with the condition when it comes from the complete hemisphere (figure 4).

The reflectance factor of the simulated soil surface with directly illuminated and

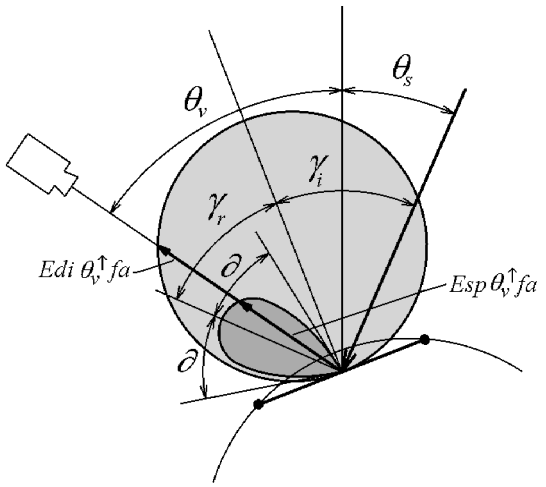

Figure 3. Distribution of the energy leaving a facet of the simulated soil surface specularly (the vector $Esp_{\theta_v{}^{\uparrow}{}_{fa}}$) and diffusely (the vector $Edi_{\theta_v{}^{\uparrow}{}_{fa}}$).

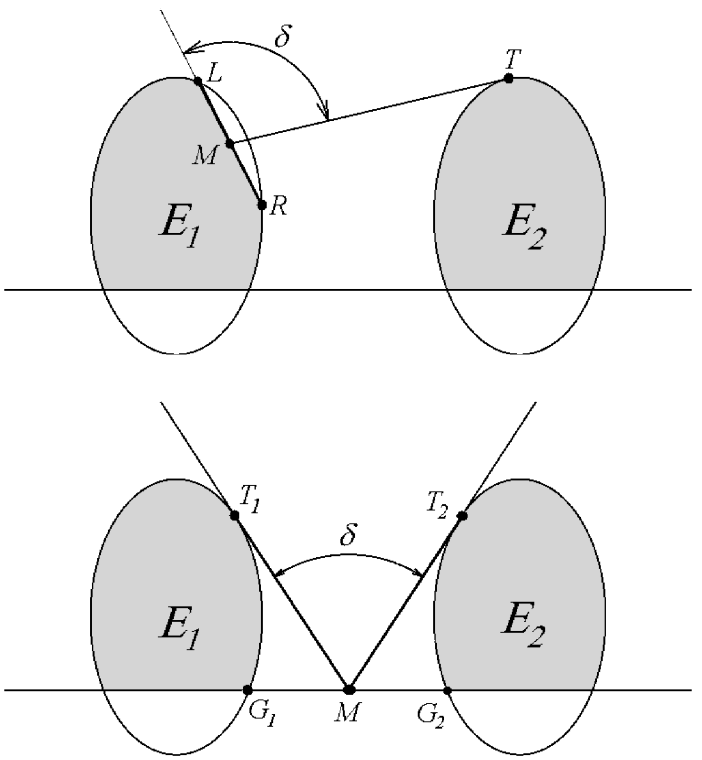

Figure 4. Limitation in illumination by diffuse light component of the facet segment LR on the ellipse E_1 ark and the slope plane between ellipses E_1 and E_2, expressed by the angle δ. M is the middle point of the segments LR and G_1G_2. T, T_1 and T_2 are the tangent points of the angle δ sides to the adjoining ellipses.

shaded fragments, viewed by the sensor from a given direction θ_v along a given profile *pr* is defined as:

$$L_{\theta_v}{}^{\uparrow}{}_{pr} = \sum_{i=1}^{j} \{(Eis_{\theta_v}{}^{\uparrow}{}_{f_{a(i)}} + Esk^{\uparrow}_{f_{a(i)}})\xi\ i_{f_{a(i)}}\} + \sum_{i=1}^{j} (Esk^{\uparrow}_{f_{a(i)}}\xi\ s_{f_{a(i)}}) \tag{2}$$

where *i* is *i*th facet of the geometrical structure, $\xi\ i_{f_{a(i)}}$ and $\xi\ s_{f_{a(i)}}$ are the elementary view angles of the illuminated and the shaded *i*th facet, respectively. The radiance of the simulated soil surface reaching the sensor through its field-of-view $L_{\theta_v}{}^{\uparrow}{}_{\mathrm{FOV}}$ is its mean values calculated along the individual profiles $L_{\theta_v}{}^{\uparrow}{}_{pr}$ and the space between the spheroids.

If the soil bidirectional reflectance modelling is applied to situations when the solar principal plane SPP crosses neither parallel to the farming direction nor perpendicular to it, the radiance of that illuminated surface $L_{(\phi_r,\ \theta_v)}{}^{\uparrow}{}_{\mathrm{FOV}}$ is calculated using the formula:

$$L_{(\phi_r,\ \theta_v)}{}^{\uparrow}{}_{\mathrm{FOV}} = L_{r\theta_v}{}^{\uparrow}{}_{\mathrm{FOV}}\left(1 - \frac{\psi}{90^\circ}\right) + L_{p\theta_v}{}^{\uparrow}{}_{\mathrm{FOV}}\frac{\psi}{90^\circ} \tag{3}$$

where $L_{r\theta_v}$ and $L_{p\theta_v}$ are the soil surface radiance calculated parallel and perpendicular to the farming direction, respectively, and ψ is the horizontal angle between the SPP and the farming direction.

Finally, the reflectance from the rough soil surface along the SPP is described by the normalized reflectance factor $NR_{(\phi_v = SPP,\ \theta_v)}$ which is defined as the ratio of the total radiance measured from the off-nadir direction θ_v to the radiance measured from nadir.

Assuming that the soil normalized reflectance factor $NR_{(\phi_v = SPP,\ \theta_v)}$ in the plane OP perpendicularly oriented to the SPP for each of the view zenith angle θ_v is 1 and the distribution of the ratio in the function of the ϕ_v between the SPP and the OP is a simple linear one, its value $NR_{(\phi_v,\ \theta_v)}$ for any observation plane can be defined as:

$$NR_{(\phi_v,\ \theta_v)} = NR_{(\phi_v = SPP,\ \theta_v)}\left(1 - \frac{\phi_v}{90^\circ}\right) + \frac{\phi_v}{90^\circ} \tag{4}$$

where ϕ_v is the relative horizontal angle of the observation plane measured from the SPP. The model was prepared in the form of computer program written in Object Pascal.

2.4. *Fitting the virtual surface geometry*

The geometry of the virtual surfaces, equivalent from an optical point of view to the real soil surfaces applied in the paper to predict their directional reflectance behaviour, was obtained by inversion of the model. The fitting of the geometrical parameters to the soil reflectance measurements involves choosing those values of the spheroid parameters, *b*, *d*, t_p, t_r, completed by the refractive index of the soil surface *n* and the ratio of the reflected diffuse light f_{di} for a given wavelength band, which gives the lowest possible *rms* error between the measured and the modelling *NR* curve. The horizontal radius of the spheroids *a*, was evaluated for a given surface as its average value estimated from the photographs. Other parameters describing conditions of illumination and observation of the studied soil surfaces, θ_s, ϕ_r, ϕ_s, *h*, α, were taken as their measured values.

This fitting was performed automatically using a special computer procedure. A program, written in Object Pascal, automatically fits the geometrical parameters of the analysed soil surfaces. It is realized in two stages. In the first one, for a surface at each illumination and observation condition, the program computes the $rms_{\theta_s,\phi_r,\phi_v,s}$, using the following formula:

$$rms_{\theta_s,\phi_r,\phi_v,s} = \frac{1}{nv-1}\sqrt{\sum_{nv-1}^{nv}(M_{\theta_s,\phi_r,\phi_v,\theta_v} - P_{\theta_s,\phi_r,\phi_v,\theta_v,s})^2} \tag{5}$$

where nv is the number of θ_v, $M_{\theta_s,\phi_r,\phi_v,\theta_v}$, is a measured value of the NR for given angles θ_s, ϕ_r, ϕ_v and θ_v, $P_{\theta_s,\phi_r,\phi_v,\theta_v,s}$ is a predicted value of NR for these angles and the set s of parameters: b, d, t_r, t_p, n and f_{di}. Those pairs, for which the measured data were collected in the situation when the radiometer cast a shadow on the observed surface, were eliminated from the calculation. In the second stage the program determines the qualities K_s:

$$K_s = \sum rms_{\theta_s,\phi_r,\phi_v,s} \tag{6}$$

where the sum is spread over all illumination and observation conditions. Finally, the minimum value among K_s is found and it indicates the set s for which the average *rms* is the lowest.

3. Results and discussion

3.1. *Soil surfaces*

Some days before the colza sowing, the soil had been ploughed up to 35 cm (Rr14). Large aggregates of the mean radius of 4.40 cm covered its surface (figure 5). Then, the soil surface was shaped by a twin farming tool, a harrow and a roll (S09). They transformed the soil into a flat and smooth surface characterized by the presence of many very small holes and some splits. The mean radius of the aggregates was 0.25 cm. One day later the seeder created furrows of a depth of 2.7 cm and a distance between their two successive tops of 15 cm, oriented at 145° to the geographic north (F10). Finally, the soil surface was formed by a heavy roller, which transformed the surface into a smooth and compact plane with aggregates of mean radius 0.35 cm (S10).

3.2. *Effects of farming works on the soil bidirectional reflectance measurements*

Results of the measurement experiment are presented in the form of normalized reflectance curves. They express the distributions of the soil surface normalized reflectance factor NR in the view zenith angle function θ_v along the solar principal plane SPP, or other observation planes, deviated from it by the horizontal angle ϕ_v (figure 6(*a*)). The curves, as in previous works of Jackson *et al.* (1990) and Cierniewski and Verbrugghe (1994), do not essentially depend on the wavelength. For each analysed soil surface, the NR data are nearly the same values for the visible bands (XS1 and XS2), as well as for the near-infrared band (XS3). For their total population, the coefficient of determination r^2 between the XS1 and the XS2, and the XS2 and XS3, reaches 0.99 and 0.98, respectively (figure 7). Taking into account these relations, variation of the normalized reflectance factor NR for one of the bands, the XS2, is discussed in the next part of this paper.

The results of our experiment, as well as others carried out by Brennan and Bandeen (1970), Kriebel (1976), Kimes and Seller (1985), Walthall *et al.* (1985), Milton and Webb (1987), and Irons and Smith (1990), show that the soil surface

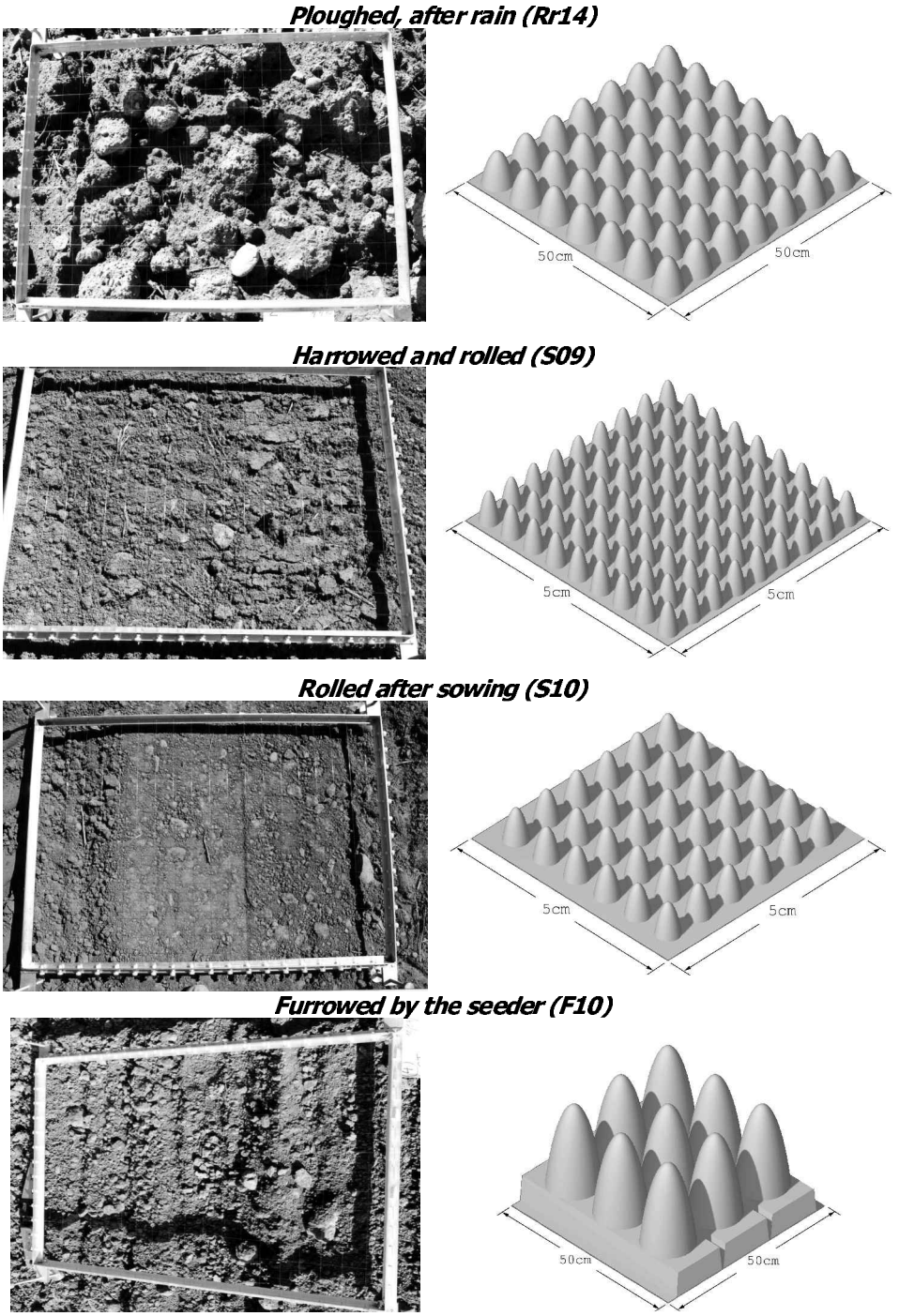

Figure 5. Photographs of the selected soil surfaces on the background of their virtual equivalents.

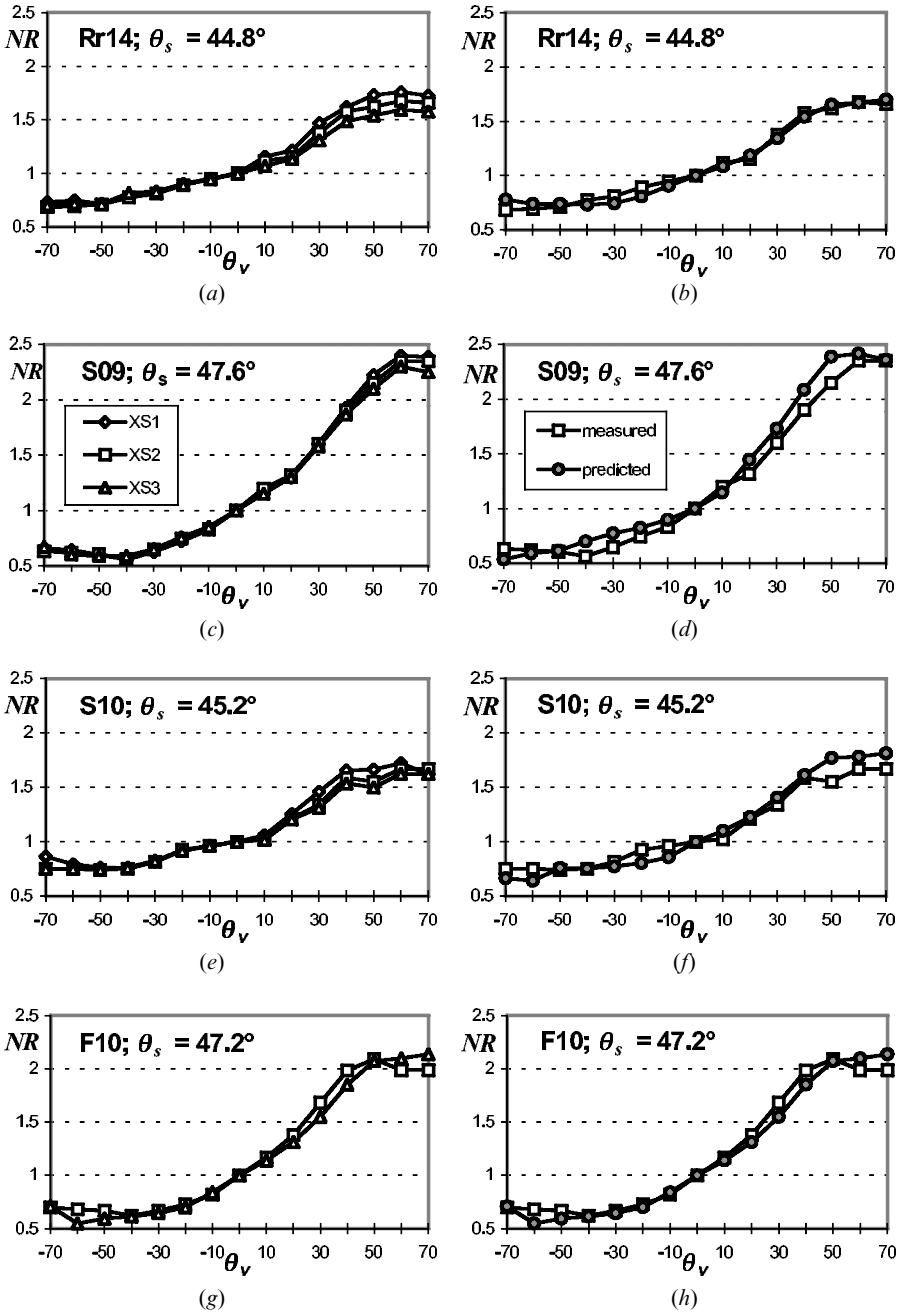

Figure 6. Normalized reflectance factor curves NR of selected soil surfaces: ploughed, after rain (Rr14), harrowed and rolled (S09), rolled after sowing (S10), and furrowed by the seeder (F10), along the solar principal plane for similar solar zenith angle θ_s values. (*a*) Measured for three channels (XS1, XS2 and XS3) and (*b*) measured and predicted by the model for the XS2 channel. Negative values of the view zenith angle θ_v correspond to forward scattering directions and positive values to backscattering directions.

$r^2 = 0.99$
$N = 471$

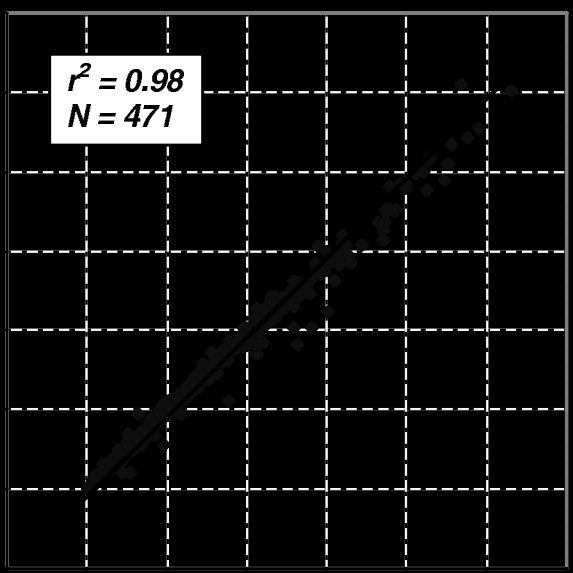

NR variation along the SPP in the view zenith angle θ_v function depends most strongly on the solar zenith angle θ_s, independent of its roughness state. To minimize the influence of the θ_s on the variation of the NR curve shape, caused by the soil surfaces roughness, only the curves for which data were collected at similar solar zenith angles can be directly analysed together, as presented in figure 6. These curves are relative to the soil surfaces roughness states resulting from four selected farming works: the ploughing (Rr14), the harrowing and rolling before sowing (S09), the furrowing by the seeder (F10) and the rolling after sowing (S10). These data were collected at θ_s between 44.8° and 47.6° along the SPP; they clearly show the effects of the soil agricultural treatments.

Two categories of the NR curves are available to distinguish among them (figure 8):

1. A relatively high NR, higher than 2 in the backscattering range, and a low NR in forward scattering directions with a minimum of about 0.6 at $-40°$ view zenith angle θ_v.
2. A clearly lower NR, reaching about 1.7 in the backscattering range and a higher NR in the forward scattering range where the NR decreases progressively to 0.5 at $-70°$ θ_v.

Both categories do not separate generally smooth soil surfaces, rolled before and after sowing, from more rough ones, i.e. deeply ploughed with rain effects and furrowed by the seeder. Generally smooth and rough soil surfaces are in the same category: the rolled before sowing (S09) and the furrowed after sowing (F10) in the first category and the rolled after sowing (S10) and the ploughed with rain effects (Rr14) in the second one. Observing more precisely the harrowed and then rolled surface before sowing (S09), belonging to the first category, it was found that generally it is smooth, although not compact enough with many small holes. These holes, causing additional irregularities of the soil surface in micro scale, are the

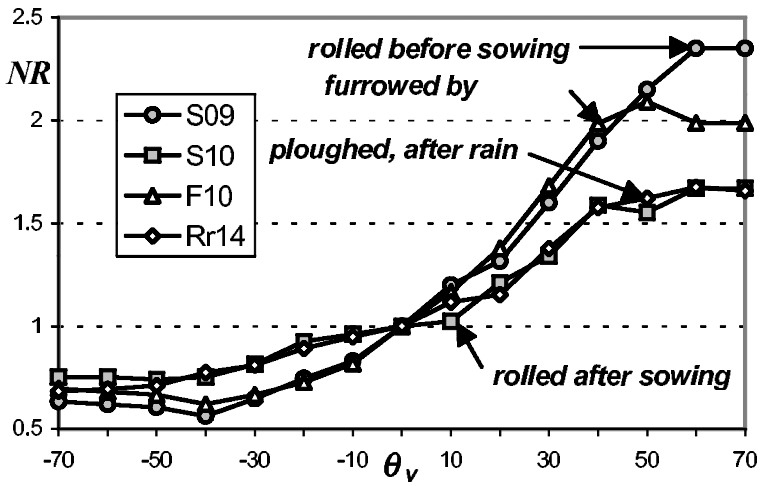

Figure 8. Selected measured normalized reflectance NR curves of the soil surfaces with roughness as the effect of different farming works: ploughed, after rain (Rr14), harrowed and rolled (S09), rolled after sowing (S10), and furrowed by the seeder (F10), for similar solar zenith angle θ_s values of about 45° at XS2 channel.

reason for the high reflectance variation along the solar principal plane of the soil surface. So, for the optical domain, the soil surface rolled before sowing (S09) behaves as a rough soil surface and its *NR* curve is similar to the curve characterizing the furrowed surface by seeder (F10). In contrast, the smooth and more compacted surface, rolled after sowing (S10), belongs to the same category as the ploughed soil after rain. A smooth crust covering the ploughed surface essentially reduces the total roughness of the soil surface for the optical domain, even with large irregularities caused by individual large clods.

The shape of the *NR* curves related to the soil surfaces with irregularities dispersed in accordance with the farming direction also depends on the relative horizontal angle ϕ_r between the direction to the Sun and the farming direction, as well as on the angle deviation ϕ_v of the observation plane from the SPP. The shape variation of the *NR* curves for gradually changing variables, describing illumination and observation conditions by the θ_s, ϕ_r and ϕ_v angles, is presented in the example of the *NR* data for the soil surface furrowed by the seeder (F10), collected just after sowing (figure 9, table 2). The surface shows clearly the increasing *NR* from forward scattering directions to the hot spot and its increase when θ_s is rising and the relative angle ϕ_r between the Sun plane and the furrows direction approaches 90°.

3.3. *Modelling of the soil surface bidirectional reflectance using virtual surfaces*

In order to obtain a quantitative description of the influence of the variables on the shape of the soil *NR* curves, the virtual soil surfaces were applied. It was assumed

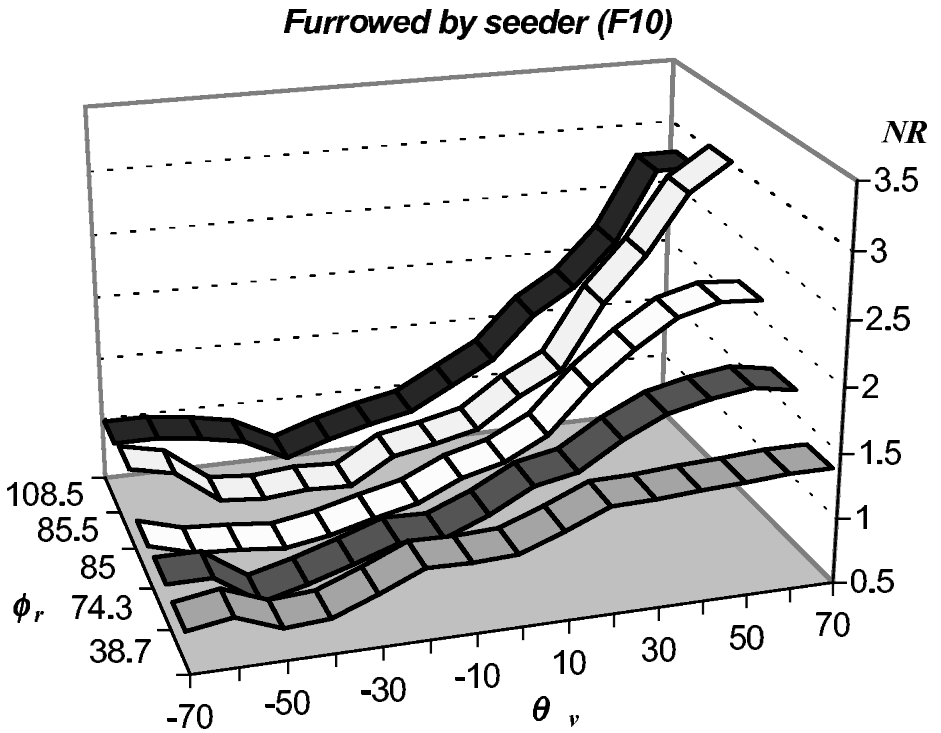

Figure 9. Normalized reflectance factor curves *NR* of the soil surface furrowed by the seeder (F10) for the XS2 band, measured for gradual changes in: the solar zenith angle θ_s, the relative horizontal angle between the Sun and the farming directions ϕ_r and the deviation angle ϕ_v of the observation plane from the solar principal plane.

that their geometrical parameters (a, b, d, t_r and t_p) are independent of the illumination and viewing conditions. In addition, the soil refractive index n for a given wavelength band is independent of the solar zenith angle θ_s. All the model-generated data were obtained with a ratio of the diffuse light of 0.05 independent of wavelengths, assuming that a higher proportion of diffuse light f_{di} in energy illuminating the target for lower wavelengths is compensated by its higher absorption for lower wavelengths after reflection. It was also assumed that the vectors of the quasi-specular component of reflected energy were visible around the direction of reflection in the angle distance ∂ equals 60°.

3.4. *Virtual soil surfaces*

The values all of these virtual surface parameters, listed in table 3, were fitted by the inversion of the model with the precision of 0.05. Some of the virtual surfaces are presented in figure 5. A large variation of the size of their spheroids is explained by the fact that these virtual surfaces are presented at different scales. All the virtual surfaces are demonstrated in the same illumination and viewing conditions.

The virtual surfaces simulating the furrowed soil surfaces (F10, Fr14, Fr16 and Fr18) are different from those simulating non-furrowed surfaces with aggregates dispersed randomly (R09, Rr14, S09, S10, Sr14). Spheroids describing these surfaces with aggregates directionally dispersed are clearly larger in size. The spheroids, sticking out from the upper plane simulate the real soil furrows, where the distance d between the spheroids directly determines the distance between the successive rows of the real furrows. The height of the virtual furrows, expressed by the t_p parameter, as well as the height of the spheroids along the furrows t_r, is about 8–10 times higher than their real equivalents. A large vertical elongation of the spheroids b/a and their relatively large heights, t_p and t_r, replace a more complicated geometry of the real soil surfaces containing very different aggregates in terms of their size and shape (Cierniewski *et al.* 1996). High values of these parameters are necessary to obtain a proper generation of *NR* curves for the cultivated soil surfaces, taking into account the geometrical assumption of the discussed model.

The size of the virtual surfaces simulating the deeply ploughed soil surfaces (R09, Rr14) in relation to the furrowed ones are about twice as small. These spheroids are

Table 3. Characteristic of the virtual soil surfaces.

Farming works	Symbol	a (cm)	b/a	d/a	t_r/a	t_p/a	t_p/t_r
Ploughed	R09	4.4	6.0	1.6	1.6	1.6	1.0
Ploughed, after rain	Rr14	4.4	5.4	1.6	1.4	1.4	1.0
Harrowed and rolled	S09	0.25	7.0	2.2	2.4	2.4	1.0
Rolled after sowing	S10	0.35	6.0	2.2	1.8	1.8	1.0
Rolled, after rain	Sr14	0.35	5.6	2.2	1.8	1.8	1.0
Furrowed by the seeder	F10	8.0	6.0	1.9	2.5	3.25	1.3
Furrowed by the seeder, after rain	Fr14	8.0	5.5	1.9	2.25	2.8	1.25
Furrowed by the seeder, after rain	Fr16	8.0	5.5	1.9	2.25	2.8	1.25
Furrowed by the seeder, after rain	Fr18	8.0	5.5	1.9	2.25	2.8	1.25

a, horizontal semi-axis of the spheroids; b, vertical semi-axis of the spheroids; d, distance between the spheroids; t_p and t_r, height of the spheroid tops above the slope plane, perpendicular and parallel to the direction of cultivation; n, the refractive index for a given wavelength: $n_{XS1} = 2.55$, $n_{XS2} = 2.50$ and $n_{XS3} = 2.48$.

also about twofold less absorbed into the slope plane, although their general shape is similar.

The spheroids describing the aggregates of the smooth soil surfaces (S09, S10 and Sr14) are more than 10 times smaller than the ploughed ones.

The spheroids of the smoothest soil surfaces (S09 and S10) are extremely vertically elongated. In relation to the ploughed virtual surfaces, they are less absorbed into the plane and are dispersed on it at about a 1.5 times larger distance d/a. The virtual S09 surface generates a very high variation of the NR in the view zenith angle θ_v function along the SPP. In contrast, the other smooth surface, S10, produces NR curves of clearly lower NR variations. The spheroids of this second virtual surface characterize their 15% smaller vertical elongation and their 1.5 times higher absorption.

The furrowed and non-furrowed virtual surfaces also allow observation of the rain effects caused by the crust, covering a thin, smoother layer of the soil surfaces after a heavy rain. In all of the examples, lower surface roughness of their real equivalents is expressed by a vertical elongation of the virtual spheroids b/a about 10% lower. The spheroids of the furrowed soil surfaces, and the ploughed one (Rr14) are additionally more absorbed, by about 10–20%, into the slope planes.

3.5. *The modelling accuracy*

The accuracy of the fitting of the b, d, t_r, t_p parameters of the virtual surfaces was evaluated analysing 32 NR curves, 16 relative to the non-furrowed surfaces and 17 to the furrowed ones, containing respectively 235 and 236 pairs of the NR data measured by the radiometer and generated by the model. The *rms* error was calculated separately for the XS1, XS2 and XS3 wavelength bands (table 4). The data for higher solar zenith angles often display a lower accuracy. The mean values of the *rms* error, calculated independently of illumination and observation conditions, yield values between 0.024 and 0.057. A higher mean accuracy was obtained for the non-furrowed surfaces: 0.030 for the XS1 and the XS2, and 0.036 for the XS3. The mean accuracy for the furrowed soil surfaces for these bands reached 0.044, 0.040 and 0.041, respectively. The lower accuracy for the furrowed soil surfaces is probably caused by the influence of the farming direction on the furrow illumination. Generating the NR for these surfaces, the additional parameter, describing the ϕ_r angle between the farming direction and the direction to the Sun, is taken into account, increasing the error of the NR prediction.

3.6. *Influence of the farming direction on the soil surface bidirectional reflectance*

The high fitting accuracy of the virtual surfaces enables us to use them as a basis for the modelling of the soil surface bidirectional reflectance for quantitative analysis of the influence of any variable on the shape of the soil NR curves. The example of the virtual surface application, the equivalent of the soil surface furrowed by the seeder (F10), to trace the influence of its farming direction in relation to the Sun position, is presented in figure 10. The influence, describing changes of the soil surface NR curve shape along the SPP, caused by the relative horizontal angle ϕ_r between the farming direction and the direction to the Sun, is analysed in the range of ϕ_r from 0° to 90° at 15° increments for three selected solar zenith angles θ_s. The model-generated NR curves show that this influence is weak. An increase of the ϕ_r angle causes a decrease of the NR in the forward scattering directions and an increase in the backscattering directions. The influence of the view geometry is the most visible

Table 4. Root mean square error for measured and model-predicted normalized reflectance NR of analysed soil surface at given roughness states.

Farming works	Symbol	Band			*rms*			mean *rms*
Harrowed and rolled	S09	θ_s (°)	*38.7*	*47.6*	*62.8*			
		XS1	0.025	0.028	0.042			0.032
		XS2	0.023	0.025	0.035			0.028
		XS3	0.033	0.045	0.042			0.040
Rolled after sowing	S10	θ_s (°)	*55.8*	*45.2*				
		XS1	0.027	0.028				0.028
		XS2	0.024	0.023				0.024
		XS3	0.032	0.034				0.033
Ploughed	R09	θ_s (°)	*37.9*	*45.5*	*60.1*			
		XS1	0.028	0.036	0.019			0.028
		XS2	0.031	0.050	0.020			0.034
		XS3	0.038	0.046	0.019			0.034
Furrowed by the seeder	F10	θ_s (°)	*67.1*	*58.1*	*47.2*	*39.9*		
		XS1	0.092	0.048	0.034	0.027		0.050
		XS2	0.081	0.053	0.021	0.024		0.045
		XS3	0.070	0.070	0.018	0.028		0.046
Furrowed by the seeder	F10	θ_s (°)	*38.2*	*45.0*	*49.5*	*59.0*	*66.3*	
		XS1	0.027	0.025	0.019	0.083	0.130	0.057
		XS2	0.025	0.040	0.025	0.061	0.094	0.049
		XS3	0.023	0.049	0.045	0.030	0.066	0.043
Furrowed by the seeder, after rain	Fr14	θ_s (°)	*40.8*	*46.6*	*52.5*	*63.3*		
		XS1	0.032	0.033	0.022	0.064		0.038
		XS2	0.035	0.028	0.028	0.058		0.038
		XS3	0.046	0.046	0.039	0.083		0.054
Ploughed, after rain	Rr14	θ_s (°)	*44.8*	*49.3*	*55.6*	*66.3*		
		XS1	0.022	0.032	0.025	0.042		0.030
		XS2	0.016	0.033	0.027	0.057		0.033
		XS3	0.022	0.031	0.029	0.058		0.035
Rolled, after rain	Sr14	θ_s (°)	*41.4*	*48.2*	*53.5*	*64.7*		
		XS1	0.025	0.024	0.033	0.051		0.033
		XS2	0.019	0.022	0.036	0.055		0.033
		XS3	0.020	0.029	0.044	0.060		0.038
Furrowed by the seeder, after rain	Fr16	θ_s (°)	*47.0*	*42.4*				
		XS1	0.026	0.045				0.036
		XS2	0.026	0.046				0.036
		XS3	0.028	0.044				0.036
Furrowed by the seeder, after rain	Fr18	θ_s (°)	*54.6*					
		XS1	0.038					0.038
		XS2	0.031					0.031
		XS3	0.026					0.026

for the solar zenith angles θ_s near 50°, when the soil surface is not shaded too much by the furrows. In this illumination condition, the increase in ϕ_r from 0° to 90° causes a decrease in NR of about 10–20% in the forward scattering range, and an increase of about 3–11% in the backscattering range. For a solar zenith angle θ_s of 30° and 70°, this NR decrease in the forward scattering range is 5–10% and 1–2%, respectively, and the increase in the backscattering range is 4–8% and 1–7%, respectively.

The virtual soil surfaces, such as those presented in the paper, can be used for re-constructing the soil bidirectional reflectance from a limited sample of angular reflectance measurements and to standardize remote sensing data collected with

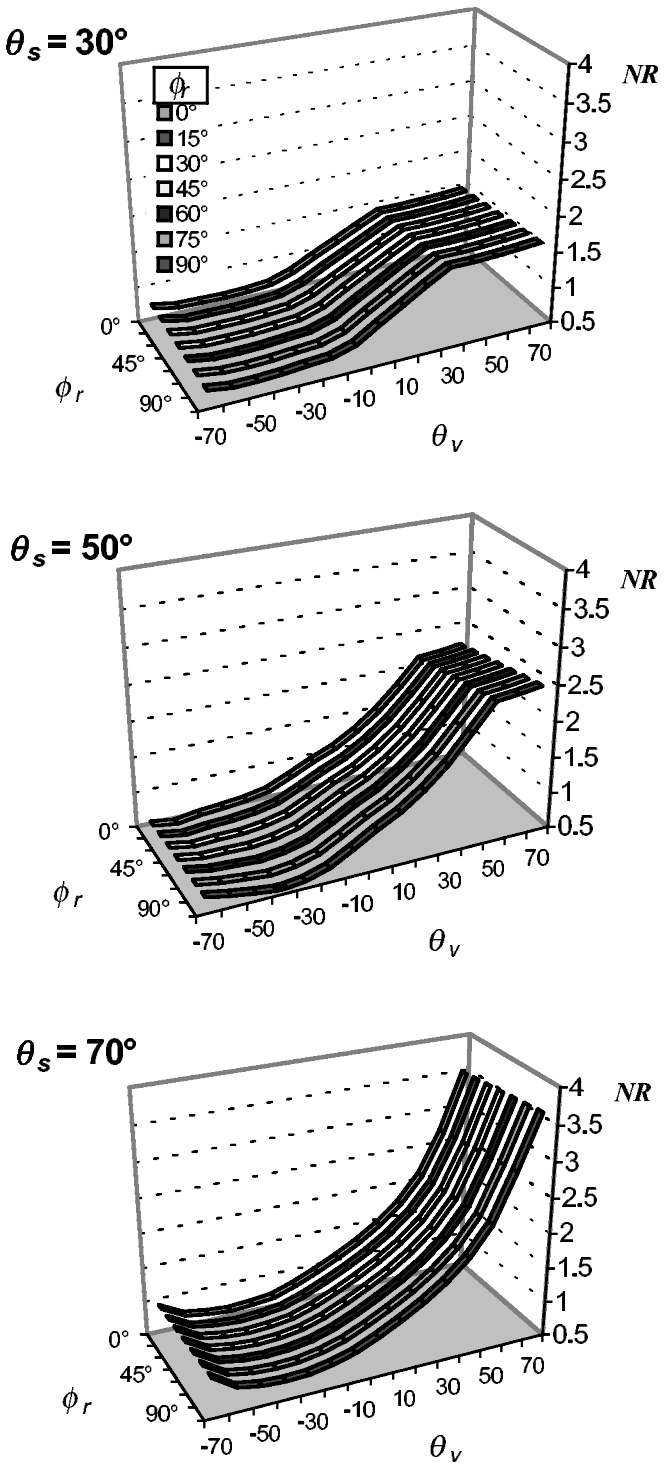

Figure 10. Normalized reflectance curves *NR* predicted by the model for the soil surface furrowed by the seeder along the solar principal plane, varying with the function of the horizontal angle ϕ_r between the farming direction and the direction to the Sun for selected solar zenith angles θ_s.

different illumination and viewing conditions. Those surfaces can be also applied to gain accurate estimates of the hemispherical reflectance and the albedo of soil surfaces.

4. Conclusions

The directional reflectance measurements in the optical domain acquired on soil surfaces with roughness (the effects of chosen farming works and heavy rain), show that the distribution of their normalized reflectance factor *NR* (defined as the ratio of the total soil radiance measured from the off-nadir direction to the radiance measured from the nadir) in the view direction function varies with soil agricultural treatment. The experimental results show that rougher soil surfaces do not always characterize a higher variation of the *NR* distribution than smooth ones. Soil surfaces smoothed by rolling can display a *NR* distribution quite similar to those of more rough surfaces, ploughed or furrowed by a seeder. As a consequence, it is difficult to predict the soil reflectance behaviour of cultivated soils taking into account their superficial structure.

The model presented in the paper, using a set of parameters describing the geometry of a soil surface and its reflectance features in the optical domain, which is a virtual surface equivalent from the optical point of view of the real rough soil surface, makes it possible to predict the soil *NR* in any illumination and viewing condition.

A virtual soil surface, supported by this model and simulating the soil surface furrowed by the seeder, has permitted us to trace the influence of the farming direction in relation to the Sun position on the soil *NR* distribution. This methodology can be used to correct remote sensing data subject to view and illumination angle effects or to retrieve albedo or hemispherical reflectance of various soil surfaces.

Acknowledgments

This work was supported by the Direction of International Relations of INRA and the Polish State Committee Scientific Research. The authors wish to thank Professor Stanislaw Bialousz (Warsaw University of Technology) for his helpful assistance during one day in the field experiment and Monsieur René Tramier, a farmer at Saint Rémy de Provence for his welcome.

References

Barnsley, M. J., 1994, Environmental monitoring using multiple-angle (MVA) remotely-sensed data. In *Environmental Remote Sensing from Regional to Global Scales*, edited by P. J. Curran and G. Foody (Chichester: John Wiley & Sons), pp. 181–201.

Brennan, B., and Bandeen, W. R., 1970, Anisotropic reflectance characteristics of natural Earth surfaces. *Applied Optics*, **9**, 405–412.

Cierniewski, J., 1987, A model for soil surface roughness influence on the spectral response of bare soils in the visible and near-infrared range. *Remote Sensing of Environment*, **123**, 97–115.

Cierniewski, J., 1999, *Geometrical Modelling of Soil Bidirectional Reflectance in the Optical Domain* (Poznan, Poland: Bogucki Scientific Publishers).

Cierniewski, J., and Verbrugghe, M., 1994, A geometrical model of soil bidirectional reflectance in the visible and near-infrared range. *Proceedings of the 6th International Symposium on Physical Measurements and Signatures in Remote Sensing, Val d'Isere, France, 17–21 January 1994*, edited by G. Guyot (Val d'Isere: C.N.E.S.), pp. 635–642.

Cierniewski, J., and Verbrugghe, M., 1997, Influence of soil surface roughness on soil bidirectional reflectance. *International Journal of Remote Sensing*, **18**, 1277–1288.

Cierniewski, J., Baret, F., Verbrugghe, M., Hanocq, J., and Jacquemud, S., 1996,

Geometrical modelling of soil bidirectional reflectance incorporating specular effects. *International Journal of Remote Sensing*, **17**, 3691–3704.

CIERNIEWSKI, J., MARLEWSKI, A., FARYS, M., and KRÓLEWICZ, S., 1998, Brightness variation of furrowed soil surfaces remotely sensed. *Quastiones Geographicae*, **19/20**, 13–22.

COOPER, K. D., and SMITH, J. A., 1985, A Monte Carlo reflectance model for soil surfaces with three-dimensional structure. *IEEE Transactions on Geosciences and Remote Sensing*, 1GE-**32**, 668–667.

IRONS, J. R., CAMPBELL, G. S., NORMAN, J. M., GRAHAM, D. W., and KOVALICK, W. M., 1992, Prediction and measurement of soil bidirectional reflectance. *IEEE Transactions on Geoscience and Remote Sensing*, **30**, 249–260.

JACKSON, R. D., TEILLET, P. M., SLATER, P. N., FEDOSEJEVS, G., JASINSKI, M. F., AASE, J. K., and MORAN, M., 1990, Bidirectional measurements of surface reflectance for view angles correction of oblique imagery. *Remote Sensing of Environment*, **32**, 189–202.

KIMES, D. S. and SELLER, P. J., 1985, Inferring hemispherical reflectance of the Earth's surface for global energy budget from remotely sensed nadir or directional radiance values. *Remote Sensing of Environment*, **18**, 205–223.

KRIEBEL, K. T., 1976, On the variability of the reflected radiation field due to differing distributions of the irradiation. *Remote Sensing of Environment*, **4**, 257–264.

MILTON, E. J., and WEBB, J. P., 1987, Ground radiometry and airborne multispectral survey of bare soils. *International Journal of Remote Sensing*, **8**, 3–14.

NORMAN, J. M., WELLES, J. M., and WALTER, E. A., 1985, Contrast among bidirectional reflectance of leaves, canopies, and soils. *IEEE Transactions on Geoscience and Remote Sensing*, GE-**23**, 659–667.

OTT, W., PFEIFFER, B., and QUIEL, F., 1984, Directional reflectance properties determined by analysis of airborne multispectral scanner data and atmospheric correction. *Remote Sensing of Environment*, **116**, 7–54.

WALTHALL, C. L., NORMAN, J. M., WALLES, J. M., CAMPBELL, G., and BLAD, B. L., 1985, A simple equation to approximate the bidirectional reflectance from vegetative canopies and bare soil surfaces. *Applied Optics*, **24**, 383–387.